Cureus Journal of Engineering
https://doi.org/10.7759/s44388-026-00289-y

Original Article

Interfacial Engineering of Polyurethane and Polymethyl Methacrylate Interpenetrating Polymer Networks using Hexaferrite Nanoceramics for Enhanced Magneto-Dielectric and Thermo-Mechanical Properties

Anil Kumar [1, ✉], Gagandeep . [1], Narendra Jakhar [2]

1. *Department of Physics, Om Sterling Global University, Hisar, IND*
2. *Department of Physics, University of Rajasthan, Jaipur, IND*

Received: May 12, 2026 | Review began: June 14, 2026 | Review ended: August 06, 2026 | Published: September 23, 2026

© **Copyright** 2026
This is an open access article distributed under the terms of the Creative Commons Attribution License CC-BY 4.0., which permits unrestricted use, distribution, and reproduction in any medium, provided the original author and source are credited.

Abstract

The present research focuses on 'Investigation of Magnetic, Mechanical, and Dielectric Properties of Hexaferrite-Modified PU/PMMA Interpenetrating Polymer Networks (IPNs)' aimed for development of multifunctional hybrid composites of Ceramic - Entangled Polymer Network represent new class of hybrid materials beneficial in advanced electronic, magnetic, mechanical, thermal and structural applications due to its flexible and foldable characteristics. In this study, IPN of polyurethane (PU) and polymethyl methacrylate (PMMA) has been prepared using sequential polymerization along with subsequently modified with controlled loadings of hexaferrite nano-ceramic ($Ba_{0.5}Sr_{0.5}Fe_{12}O_{19}$) act as inorganic fillers. Due to high magneto-crystalline anisotropy, thermal stability, and dielectric tenability of hexaferrites results in in considering the $Ba_{0.5}Sr_{0.5}Fe_{12}O_{19}$ as a potential candidate for various application. The homovalent modification (Different atomic radii) enhances magnetic and dielectric behavior. For this, nano-sized $Ba_{0.5}Sr_{0.5}Fe_{12}O_{19}$ hexaferrite ceramics has been prepared with auto-combustion method using nitrates of various metal ions required as per according to stoichiometry mentioned above. The sintered powder of prepared hexaferrite nano-ceramics has been incorporated in matrix of PU/PMMA IPN during In-situ polymerization and comprehensive characterization techniques, like Fourier-transform infrared spectroscopy, X-ray diffraction, scanning electron microscopy, vibrating-sample magnetometry, universal testing machine, dielectric spectroscopy, and impedance analysis have been employed to evaluate the structural, morphological, magnetic, mechanical, and dielectric behavior of the prepared composites. The incorporation of hexaferrite nanoparticles significantly improved magnetic behavior while maintaining structural integrity. Presence of ceramic in matrix of PU-PMMA has been confirmed first from X-ray diffraction peaks appears in Hexaferrite-Modified PU/PMMA IPNs. Morphological analysis has been carried out using scanning electron microscopy in field emission mode. Establishment of magnetic response in non-magnetic PU-PMMA entangled interpenetrating polymer network has been verified from Magnetization vs. Magnetic hysteresis curve. Improved heat resistance response of PU-PMMA entangled interpenetrating polymer network due to incorporation of $Ba_{0.5}Sr_{0.5}Fe_{12}O_{19}$ hexaferrite nanoparticles has been confirmed from Thermo-Gravimetric curve also signature for influence of $Ba_{0.5}Sr_{0.5}Fe_{12}O_{19}$ hexaferrite ceramics weight loss of IPN, whereas ε'& ε" vs. Frequency shows modification in dielectric properties due to $CoFe_2O_4$. The influence of $Ba_{0.5}Sr_{0.5}Fe_{12}O_{19}$ hexaferrite ceramics in matrix of PU-PMMA entangled interpenetrating polymer network further studied from Tensile strength (Elongation at beak) and hardness calculated using Instron tensile tester and Rockwell hardness tester. ε′, ε˝& σac vs. Frequency at room temperature reveals effect of $Ba_{0.5}Sr_{0.5}Fe_{12}O_{19}$ hexaferrite ceramics in

How to cite this article:
Kumar A, . G, Jakhar N (September 23, 2026) Interfacial Engineering of Polyurethane and Polymethyl Methacrylate Interpenetrating Polymer Networks using Hexaferrite Nanoceramics for Enhanced Magneto-Dielectric and Thermo-Mechanical Properties. Cureus J Eng 3 : es44388-026-00289-y. DOI https://doi.org/10.7759/s44388-026-00289-y

matrix of PU-PMMA entangled interpenetrating polymer network on dielectric properties, whereas fitting of dielectric data shows extent of deviation from normal Debye behavior.

Categories: Nano Materials, Nanotechnology, Polymer Science and Engineering

Keywords: hexaferrite, inorganic filler, interpenetrating polymer network (ipn), tensile strength, magnetic hysteresis loop, dielectric permitivity

Introduction

In recent days, polymers due to their environmentally favorable behavior and cost-effective synthesis gain lots of attention from researchers in both academic as well as R&D sections in various industries, but strength and other important properties such as electrical and magnetic response put the polymers back end. A new class of approach such as entanglement of two polymers by cross-linking and using fillers (Organic as well as Inorganic) results in resolving such issues. Interpenetrating polymer networks (IPNs) are such kind of polymers that have attracted significant attention in recent years due to their thermal and mechanical enhancement and ability to combine advantageous properties of two or more polymeric systems without macroscopic phase separation in a single polymer. Among various IPN architectures such as PU-Pani, PU-HEMA, etc., interpenetrating polymer network of Polyurethane (PU) and Poly(methyl methacrylate) (PMMA) based IPNs are particularly appealing owing to the complementary nature of their properties [1-7].

IPNs have attracted significant attention in recent years due to their unique ability to combine the advantageous properties of two or more polymeric systems without macroscopic phase separation. Among various IPN architectures, PU and PMMA based IPNs are particularly appealing owing to the complementary nature of their properties. PU provides elasticity, toughness, and impact resistance, while PMMA contributes rigidity, transparency, and good dielectric stability. The formation of a PU/PMMA IPN thus enables tailored mechanical and functional performance suitable for advanced structural and electronic applications. The incorporation of functional inorganic fillers into polymer IPNs has emerged as an effective strategy to further enhance and tune their physical properties. Hexaferrites, especially M-type hexaferrites, are technologically important magnetic ceramics known for their high coercivity, chemical stability, moderate saturation magnetization, and excellent dielectric behavior at high frequencies. These characteristics make hexaferrites promising candidates for applications in electromagnetic interference (EMI) shielding, microwave absorption, sensors, and multifunctional polymer composites. Embedding hexaferrite particles within a PU/PMMA IPN matrix offers the possibility of synergistically integrating magnetic, mechanical, and dielectric functionalities within a single material system. The interpenetrated polymeric structure can restrict filler agglomeration, improve filler-matrix interfacial interactions, and facilitate effective stress transfer, thereby influencing the overall performance of the composite. Moreover, the presence of hexaferrite particles can significantly modify the dielectric polarization mechanisms and magnetic response of the polymer network under an applied field. Despite growing interest in ferrite-polymer composites, systematic studies addressing the simultaneous influence of hexaferrite incorporation on the magnetic, mechanical, and dielectric response of PU/PMMA IPNs remain limited. Understanding the structure-property relationships in such hybrid systems is essential for designing next-generation multifunctional materials [8-12].

PU provides elasticity, toughness, and impact resistance, while PMMA contributes rigidity, transparency, and good dielectric stability. The formation of a PU/PMMA IPN thus enables tailored mechanical and functional performance suitable for advanced structural and electronic applications [13-16]. The incorporation of functional inorganic fillers into polymer IPNs has emerged as an effective strategy to further enhance and tune their physical properties. Hexaferrites, especially Since in M-type hexaferrite, the structure has five distinct crystallographic interstitial sites, labeled as three octahedral sites (12k, 2a, 4f2), one tetrahedral site (4f1), and one trigonal bipyramidal site (2b). The octahedral positions within the crystal structure are occupied by Fe^{3+} ions with their spins aligned in the same direction (spin-up) contributing to the magnetic properties of the material. The 12k, 2a, and 2b sites are considered "spin-up" sites, while the 4f1 and 4f2 sites are "spin-down" sites. There are two formula units per unit hexagonal unit cell of hexaferrite, wherein 12 Fe^{3+} ions are distributed in these interstitial sites. There are six ions with upward spin alignment in the 12k, one in 2a and one in 2b

sites, with a total of eight Fe^{3+} ions with upward spin alignment and there are two ions each in the 4f1 and 4f2 sites, with their downward spin alignment. So, up-spins of four ions cancel out down-spins of four ions and the net magnetic moment accounts for the upward spins of four Fe^{3+} ions. There are only spin contributions to the magnetic moment of each Fe^{3+} ion, containing five unpaired d-electrons, accounting for a magnetic moment of 5.92 Bohr magneton per ion calculated as

$$\mu_s = \sqrt{n\,(n+2)}$$

Where 'n' is the number of un-pair (05) electrons in d-orbitals of Fe^{3+} ion.

Therefore, total magnetic moment per formula unit containing 12 Fe^{3+} ions with spin upward alignment of remaining four ions is 23.68 Bohr magneton and hence of unit cell of hexaferrite containing 24 Fe^{3+} ions is 47.36 Bohr magneton [17-24].

In this work, we report a comprehensive study on the magnetic, mechanical, and dielectric behavior of hexaferrite-modified PU/PMMA interpenetrating polymer networks. The effect of hexaferrite loading on magnetization characteristics, tensile properties, and dielectric parameters has been investigated in detail, and the underlying mechanisms governing the observed responses are discussed.

Materials And Methods

Experimental methodology

Multifunctional hybrid composites of Ceramic - Entangled Polymer Network in the form of thin foldable sheets of $Ba_{0.5}Sr_{0.5}Fe_{12}O_{19}$ Hexagonal ferrite nanoparticles incorporated in the matrix of PU-PMMA Entangled Polymer Network have been synthesized using in-situ polymerization of $Ba_{0.5}Sr_{0.5}Fe_{12}O_{19}$ and PU and methyl methacrylate (MMA). For such preparation, $Ba_{0.5}Sr_{0.5}Fe_{12}O_{19}$ was first synthesized using auto-combustion of nitrates of metal dissolved in water along with a fuel agent (Citric Acid). For this, first metal nitrates mentioned in stoichiometric proportion have been weighed and dissolved in DDI and magnetically stirred for homogenous mixing with simultaneous heating until combustion starts and ends with fine powder as the final product at a pH value maintained at ~7 to ~8 using liquid ammonia solution. The powder has been calcined at 950°C for 12 hours and then sintered in the form of pellets (Uniform Mixture of Calcined Powder with 4% wt Polyvinyl Alcohol) at 1250°C for 2 hours. The pellets have been crushed into powder and heated at 500°C for 2 hours for removal of strain produced during crushing of pellets using motar and pestle. For preparation of PU-PMMA IPN incorporated with $Ba_{0.5}Sr_{0.5}Fe_{12}O_{19}$, Flexible Mats of 1-_x (PU/PMMA IPN)-$_x(Ba_{0.5}Sr_{0.5}Fe_{12}O_{19})$, where x = 20%, 30%, 40% wt have been made using in-situ polymerization. For preparation of IPN of PU and Polystyrene (PMMA), first polymerization of Castor oil and MDI (Methyl Diisocyanate) in 1:1 equivalent weight has been carried out resulting in PU. During polymerization process, MMA (act as Monomer for PMMA) has been dissolved simultaneously along with The N,N-dimethyl aniline and benzoyl peroxide. The ferrite powder has also dissolve along N, N dimethyl aniline and benzoyl peroxide using high shear homogenizer and ultra-sonication. The N, N dimethyl aniline (as a catalyst) and benzoyl peroxide (Chain Initiator) have been used for IPN Flexible Mats of x(PU/PMMA IPN)- 1-x($Ba_{0.5}Sr_{0.5}Fe_{12}O_{19}$) and characterized with various technique like Fourier-transform infrared spectroscopy (FTIR), X-ray diffraction (XRD), scanning electron microscopy (SEM), vibrating-sample magnetometry (VSM), thermogravimetric analysis (TGA), universal testing machine (UTM), dielectric spectroscopy, and impedance analysis have been employed to evaluate structural, morphological, magnetic, mechanical, and dielectric behavior of the prepared composites.

How to cite this article:
Kumar A, . G, Jakhar N (September 23, 2026) Interfacial Engineering of Polyurethane and Polymethyl Methacrylate Interpenetrating Polymer Networks using Hexaferrite Nanoceramics for Enhanced Magneto-Dielectric and Thermo-Mechanical Properties. Cureus J Eng 3 : es44388-026-00289-y. DOI https://doi.org/10.7759/s44388-026-00289-y

Results And Discussion

The successful formation of hexagonal ferrite nanoparticles incorporated into the PU-PMMA foldable sheet has also been identified from XRD data. XRD data actually reveals the presence of crystalline nature in the interpenetrating polymer network. Structural phase analysis of hexagonal ferrite nanoparticles ($Ba_{0.5}Sr_{0.5}Fe_{12}O_{19}$) incorporated in the matrix of PU-PMMA IPN has been investigated using XRD data. Sharp and high-intensity diffraction peaks signify the crystalline behavior of hexagonal ferrite nanoparticles ($Ba_{0.5}Sr_{0.5}Fe_{12}O_{19}$) present in the matrix of PU-PMMA IPN. XRD data of hexagonal ferrite nanoparticles ($Ba_{0.5}Sr_{0.5}Fe_{12}O_{19}$) has been displayed in Figure *1* (a-d). Figure *1* (a) shows XRD pattern of $Ba_{0.5}Sr_{0.5}Fe_{12}O_{19}$ ferrite nanoparticles incorporated in the matrix of PU-PMMA foldable sheet with wt% of ferrite nanoparticle of 20%, 30% and 40%, whereas in Figure *1* (b), XRD pattern from 2θ ~ 30°- 40° of $Ba_{0.5}Sr_{0.5}Fe_{12}O_{19}$ ferrite nanoparticles incorporated in the matrix of PU-PMMA foldable sheet with wt% of ferrite nanoparticle of 20%, 30%, and 40% and Figure *1* (c) represents diffraction pattern from 2θ ~ 30°- 40° of $Ba_{0.5}Sr_{0.5}Fe_{12}O_{19}$ ferrite nanoparticles incorporated in the matrix of PU-PMMA foldable sheet with wt% of ferrite nanoparticle of 40%, whereas Figure *1* (d) shows diffraction pattern of $Ba_{0.5}Sr_{0.5}Fe_{12}O_{19}$ ferrite nanoparticles from 2θ ~ 20°- 80°. The broad hump in 2θ ~ 10°-20° reveals the presence of polymer like behavior confirms PU-PMMA interpenetrating polymer network, whereas high-intensity sharp diffraction peaks confirm the establishment of crystalline behavior due to incorporation of inorganic filler ($Ba_{0.5}Sr_{0.5}Fe_{12}O_{19}$ ferrite nanoparticles) in the matrix of PU-PMMA IPN. It has also been clear from the figure that as the content of ferrite nanoparticle as filler increases (wt%), the broad hump disappears continuously and in x = 40%, it disappears completely, revealing the dominance of crystalline behavior over amorphous behavior of PU-PMMA IPN, also establishing the solid dispersing limit in the matrix of polymer. The analysis of crystalline behavior of PU-PMMA IPN due to incorporation of inorganic filler ($Ba_{0.5}Sr_{0.5}Fe_{12}O_{19}$ ferrite nanoparticles) has been studied by comparing the position of diffraction peaks that appear in PU-PMMA IPN and comparing XRD data which were experimentally collected at room temperature with diffraction data of hexaferrite reported in the literature as well as with JCPDS card.

Experimentally collected data of $_{x}$(PU/PMMA IPN)- $_{1-x}$($Ba_{0.5}Sr_{0.5}Fe_{12}O_{19}$ Hexagonal ferrite nanoparticles, where x = 20%, 30%, and 40% of hexaferrites, has been investigated using JCPDS card no. 79-1411 stamped for the appearance of hexagonal crystal phase of $SrBaFe_{12}O_{19}$ {M-type hexaferrite (Space Group P63/mmc No. 194)}, respectively. Diffraction peaks appear at 2θ ~ 32.41 and 34. 23 in experimentally collected data of foldable sheet and confirm the presence of hexagonal structural phase of M-type hexaferrite ($SrBaFe_{12}O_{19}$), whereas broad diffraction peak from 2θ ~12° to 20° must be due to polymer nature of PU-PMMA IPN.

How to cite this article:
Kumar A, . G, Jakhar N (September 23, 2026) Interfacial Engineering of Polyurethane and Polymethyl Methacrylate Interpenetrating Polymer Networks using Hexaferrite Nanoceramics for Enhanced Magneto-Dielectric and Thermo-Mechanical Properties. Cureus J Eng 3 : es44388-026-00289-y. DOI https://doi.org/10.7759/s44388-026-00289-y

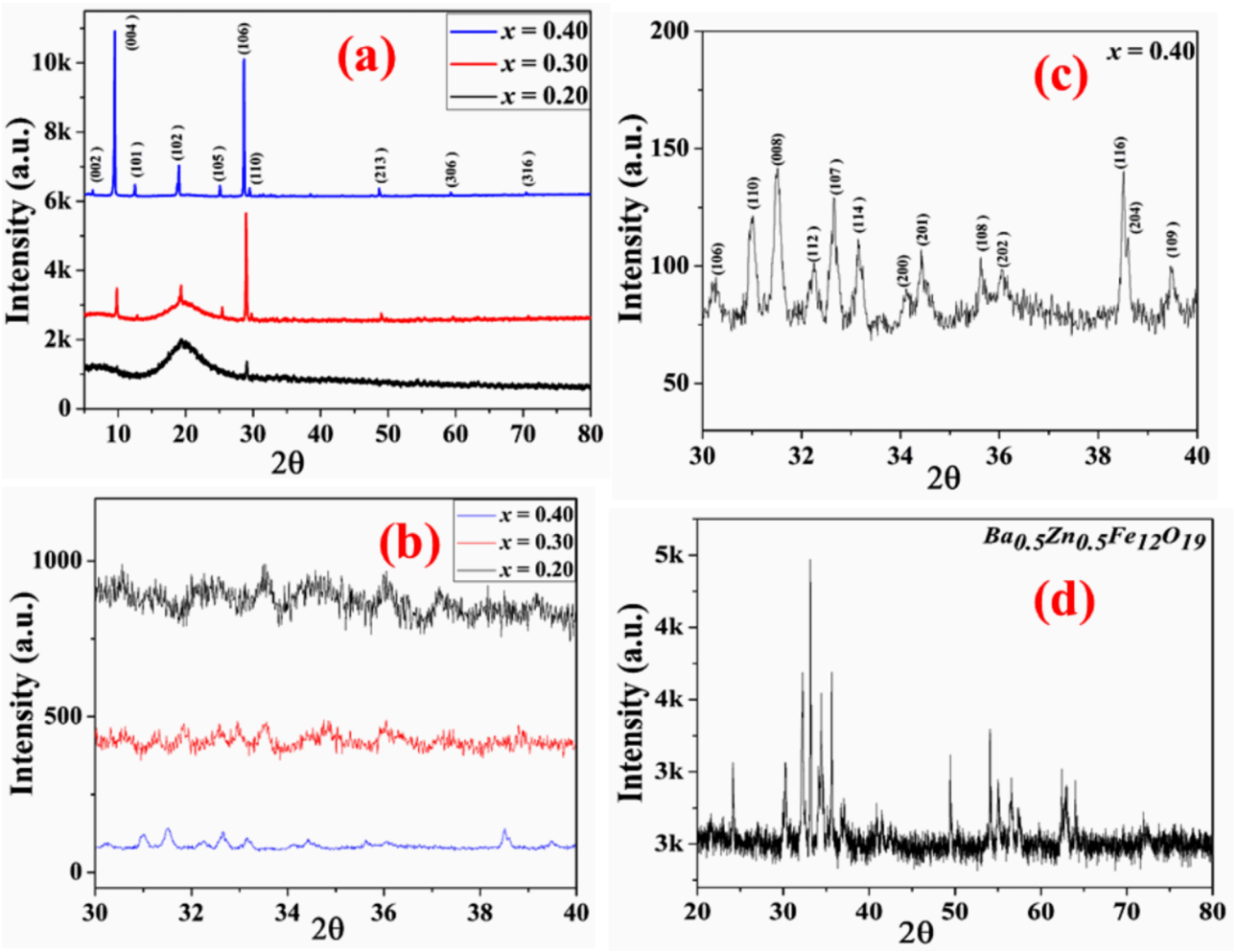


FIGURE 1: (a) X-ray diffraction of flexible mats of x(PU/PMMA IPN)-1-x(Ba0.5Sr0.5Fe12O19 hexagonal ferrite nanoparticles), where x = 20%, 30%, 40%; (b) X-ray diffraction of flexible mats of x(PU/PMMA IPN)-1-x(Ba0.5Sr0.5Fe12O19, x = 20%, 30%, 40% from 2θ ~ 30°–40°); (c) diffraction of flexible mats of x(PU/PMMA IPN)-1-x(Ba0.5Sr0.5Fe12O19, x = 40% wt from 2θ ~ 30°–40°); and (d) diffraction of Ba0.5Sr0.5Fe12O19 hexagonal ferrite nanoparticles

PU, Polyurethane; PMMA, Polymethyl Methacrylate; IPN, Interpenetrating Polymer Network

To further analyze the crystal structure and investigate the effect of structure-property relation like the effect of non-crystalline behavior of PU-PMMA IPN and crystalline nature of hexagonal ferrite incorporated in the matrix of polymer, the peak position of diffraction peaks appearing in flexible and foldable mats of $_{x}$(PU/PMMA IPN)-$_{1-x}$($Ba_{0.5}Sr_{0.5}Fe_{12}O_{19}$ x = 40% wt (With maximum loading of $Ba_{0.5}Sr_{0.5}Fe_{12}O_{19}$ nanoparticle in matrix of IPN)) from 2θ ~ 30°- 40° has been compared with the peak position reported in JCPDS card of hexagonal ferrite and reported in Table *1*.

How to cite this article:
Kumar A, . G, Jakhar N (September 23, 2026) Interfacial Engineering of Polyurethane and Polymethyl Methacrylate Interpenetrating Polymer Networks using Hexaferrite Nanoceramics for Enhanced Magneto-Dielectric and Thermo-Mechanical Properties. Cureus J Eng 3 : es44388-026-00289-y. DOI https://doi.org/10.7759/s44388-026-00289-y

2θ for x = 40%	hkl
30.265 (29.177)	106
31.019 (30.400)	110
31.502 (31.140)	008
32.227 (31.405)	112
32.644 (32.451)	107
33.141 (34.260)	114
34.136 (35.245)	200
34.415 (35.468)	201
35.600 (35.896)	108
36.068 (36.130)	202
38.519 (38.506)	116
38.608 (38.679)	204
39.493 (39.484)	109

TABLE 1: 2θ and their corresponding "hkl" of flexible mats of x(PU/PMMA IPN)-1-x(Ba0.5Sr0.5Fe12O19 hexagonal ferrite nanoparticles, where x = 40%)

PU, Polyurethane; PMMA, Polymethyl Methacrylate; IPN, Interpenetrating Polymer Network

A considerable shift has been clearly visualized from Table *1* in the position of diffraction peak when compared with diffraction data reported in the above-mentioned JCPDS card no. 79-1411. The miller indices (hkl) reported in Table *1* (red colored according to the reported in JCPDS card no. 79-1411), whereas in black color corresponds to experimentally collected data. This difference in the position of diffraction peak of flexible mats of $_{x}$(PU/PMMA IPN)-$_{1-x}$($Ba_{0.5}Sr_{0.5}Fe_{12}O_{19}$ hexagonal ferrite nanoparticles, where x = 40%) in comparison with the peak position of JCPDS card no. 79-1411 may be a result of changes in crystal parameters (lattice parameters, crystallite size (D), micro strain (ε) as well as dislocation density (δ) and others).

The lattice parameter of hexagonal crystal phase of fexible mats of $_{x}$(PU/PMMA IPN)- $_{1-x}$($Ba_{0.5}Sr_{0.5}Fe_{12}O_{19}$ hexagonal ferrite nanoparticles, where x = 20%, 30%, 40%) have been calculated using Equation (1) [25,26]:

$$\frac{1}{d_{hkl}^2} = \frac{4}{3}\left(\frac{h^2 + hk + k^2}{a^2}\right) + \frac{l^2}{c^2} (1)$$

Where h, k and l are miller indices and "a" and "c" are lattice constants and unit cell of hexagonal crystal system has been calculated using Equation (2)

$$V = \left(a^2 c\right) \sin 120^\circ \, (2)$$

The lattice constants (a and c) evaluated by using these equations and Bragg's diffraction law as well as unit cell volume calculated using above mentioned equation are reported in Table 2.

Composition↓ Crystal Phase→	**Hexagonal Space Group $P6_3/mmc$ No. 194**			
Crystal Parameter	a(Å)	c(Å)	D (nm)	V($Å^3$)
x = 0.20 %wt	5.903	23.083	70.770	696.555
x = 0.30 %wt	5.906	23.107	69.550	697.988
x = 0.40 %wt	5.914	22.979	114.90	696.003

TABLE 2: Crystallographic investigations such as lattice parameters (a and c) of flexible mats of x(PU/PMMA IPN)-1-x(Ba0.5Sr0.5Fe12O19 hexagonal ferrite nanoparticles, where x = 20%, 30%, 40%)

PU, Polyurethane; PMMA, Polymethyl Methacrylate; IPN, Interpenetrating Polymer Network

Table 2 clearly reveals that a slight change in lattice parameters (a and c [Å]) may result due to variations in stoichiometric concentration as well as distribution in the matrix of polymer because during performing experiments, diffraction may result in change in the position of diffraction peaks due to the amorphous response of the polymer behavior of entangled polymer, which is maximum in stoichiometric proportion.

The further investigation of crystalline signatures such as crystallite size (D: Calculated using Debye-Scherrer's formula), micro strain (ε) and dislocation density (δ) have been calculated using formulae given below: Equation (3)

$$D = \frac{0.9\lambda}{\beta \cdot \cos\theta} (3)$$

Micro strain (ε) and Dislocation density (δ)

$$\epsilon = \frac{\beta \cos\theta}{4} (4)$$

$$\delta = \frac{1}{D^2} (5)$$

where λ = 1.54 Å is the wavelength of the X-ray beam used in X-ray diffractometer, β is FWHM of XRD data peak and θ is Bragg's angle of diffraction, as reported in Table 3.

Composition↓ Crystal Phase→	Hexagonal Space Group $P6_3/mmc$ No. 194	
Crystal Parameter	ε	δ [$Å^{-2}$]
x = 0.20 %wt	0.00174	1.996 E-4
x = 0.30 %wt	0.00167	2.067 E-4
x = 0.40 %wt	0.0011	7.574 E-5

TABLE 3: Macro-strain, dislocation of flexible mats of x(PU/PMMA IPN)-1-x(Ba0.5Sr0.5Fe12O19 hexagonal ferrite nanoparticles, where x = 20%, 30%, 40%)

PU, Polyurethane; PMMA, Polymethyl Methacrylate; IPN, Interpenetrating Polymer Network

Average crystallite size calculated using Debye-Scherrer's formula indicates that inorganic filler in the matrix of entangled polymer crystallizes in nanosized and slightly decreases in dislocation density also from 1.996 E-4 to 7.574 E-5, and this decrease in microstrain and dislocation density may result in a large difference in the c-axis of both hexagonals.

Microstructural characteristics of $_x$(PU/PMMA IPN)-$_{1-x}$($Ba_{0.5}Sr_{0.5}Fe_{12}O_{19}$ hexagonal ferrite nanoparticles, where x = 20%, 30%, 40% , and 50%wt) have been shown in Figure *2* (a-d). Figure *2*(a) shows microstructure of $_x$(PU/PMMA IPN)-$_{1-x}$($Ba_{0.5}Sr_{0.5}Fe_{12}O_{19}$ Hexagonal ferrite nanoparticles, where x = 40%), (b) x = 30%, (c) x = 20%, and (d) $Ba_{0.5}Sr_{0.5}Fe_{12}O_{19}$ hexagonal ferrite nanoparticles. The micrographs were taken at the same applied voltage (5kV) and magnification (100 KX) using a field emission signal for generation of the electron beam in the scanning electron microscope. The white region in micrographs reveals $Ba_{0.5}Sr_{0.5}Fe_{12}O_{19}$ hexagonal ferrite nanoparticles of ceramics in PU-PMMA foldable flexible mats, whereas cross-linked non-uniform and irregular grains in Figure *2* (d) show non-uniformly distributed hexagonally shaped grains of ceramic oxide that act as filler to improve mechanical enhancement of entangled cross-linked polymer. Micrographs also point toward agglomeration of smaller grains due to magnetic interaction between the individual grains of the prepared samples. The extent of cross-linked grains shows grain growth and irregular shaped and sized cross linked grains along with some porous like structure that confirms uniform dispersion of ferrite particles in the matrix of PU/PMMA IPN.

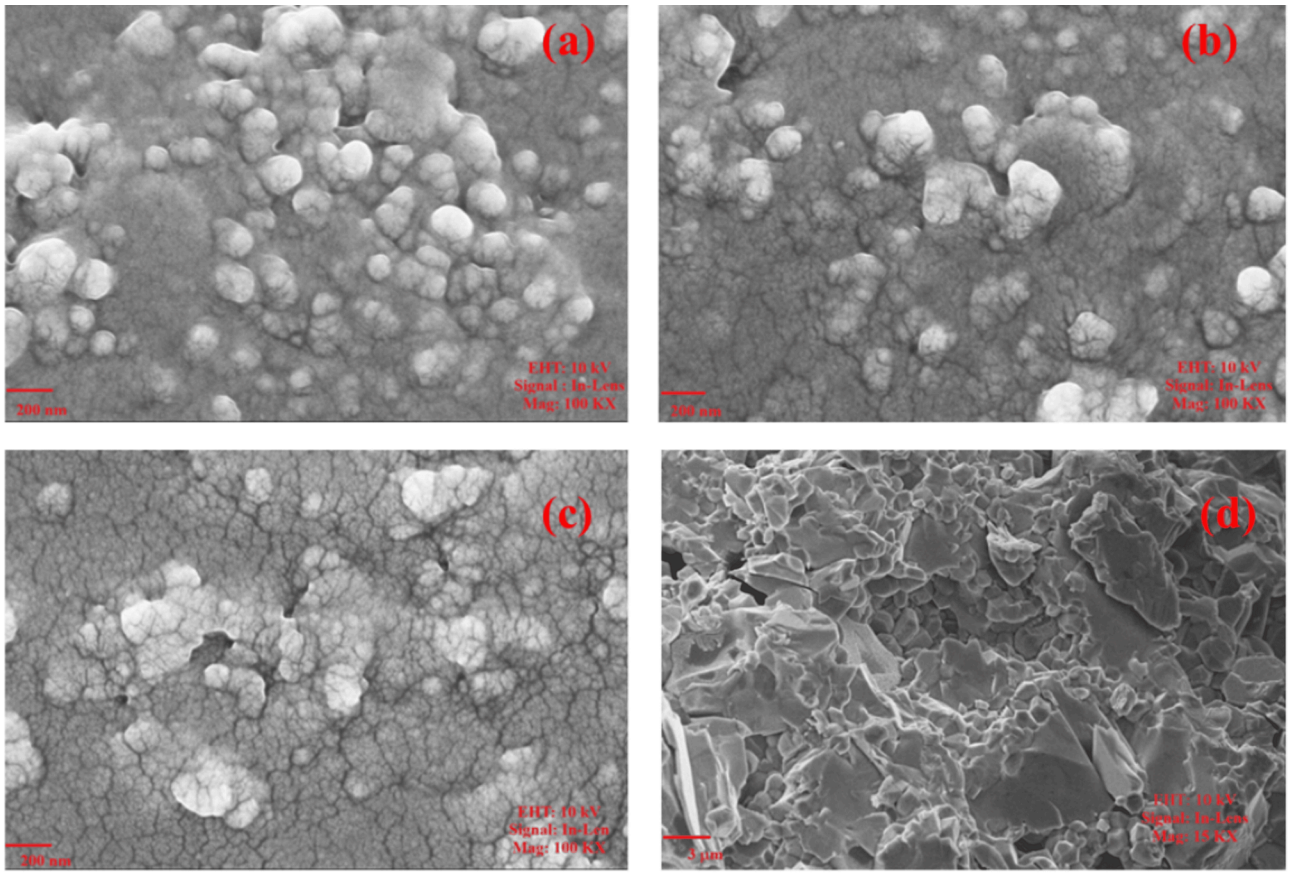


FIGURE 2: FESEM micrographs of flexible mats of x(PU/PMMA IPN)-1-x(Ba0.5Sr0.5Fe12O19 hexagonal ferrite nanoparticles, (a) x = 40%, (b) x = 30%, and (c) x = 20%, and (d) Ba0.5Sr0.5Fe12O19 hexagonal ferrite nanoparticles

PU, Polyurethane; PMMA, Polymethyl Methacrylate; IPN, Interpenetrating Polymer Network; FESEM, Field-Emission Scanning Electron Microscopy

FTIR spectra of flexible mats of $_{x}$(PU/PMMA IPN)- $_{1-x}$($Ba_{0.5}Sr_{0.5}Fe_{12}O_{19}$ hexagonal ferrite nanoparticles, x = 40%) have been shown in Figure *3* in transmittance mode. Si-OH and OH stretching has been confirmed from peak position of transmittance peaks around wave no. ~3324 cm^{-1}, whereas the peak positioned at ~2924 and 2852 cm^{-1} reveals asymmetric and symmetric vibration of the methylene group (CH_2) due to the aliphatic carbon chain. The position of peaks at ~1750 to 1730 and ~1360 to 1180 cm^{-1} responds toward the presence of carbonyl C=O stretching of free urethane as well as C-N stretching along with Si-O-Si stretching at ~1040-1050 cm^{-1} corresponds. Tetrahedral vibrational stretching is confirmed from the peak positioned at ~570 and 538 cm^{-1} and results from Fe and O, whereas the peak positioned at ~420 cm^{-1} reveals octahedral stretching that is evident for the presence of M-type hexagonal structure in flexible PU-PMMA IPN sheets [27,28].

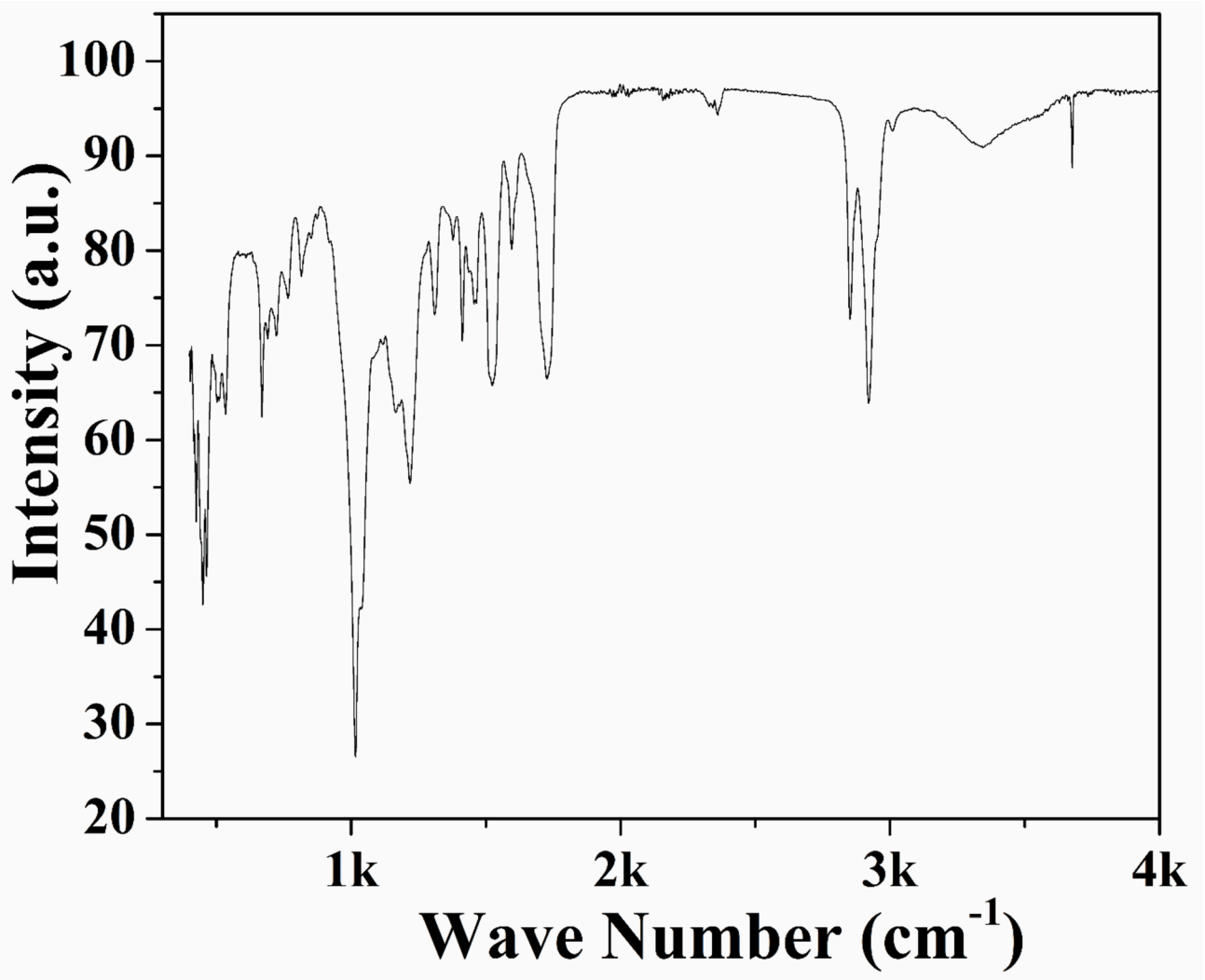


FIGURE 3: FTIR spectra of flexible mats of x(PU/PMMA IPN)-1-x(Ba0.5Sr0.5Fe12O19 hexagonal ferrite nanoparticles, x = 40%)

PU, Polyurethane; PMMA, Polymethyl Methacrylate; IPN, Interpenetrating Polymer Network; FTIR, Fourier-Transform Infrared Spectroscopy

Establishment of magnetic signature in nonmagnetic interpenetrating polymer network has been investigated from Magnetization vs. Magnetic curve recorded at room temperature using VSM with an applied strength of magnetic field of 1.5±Tesla. M vs. H magnetic hysteresis curve of $_x$(PU/PMMA IPN)-$_{1-x}$($Ba_{0.5}Sr_{0.5}Fe_{12}O_{19}$ Hexagonal ferrite nanoparticles, where x = 20%, 30%, 40%, and 50%wt). Magnetic properties at room temperature have been shown in Figure *3*. Nonlinear S-shaped curve in 1 and 3 quadrant stamps the establishment of magnetic character in nonmagnetic PU-PMMA IPN. Figure *4* displays (a) Magnetization vs. Applied Magnetic Field and (b) Variation of remnant magnetization (M_r), Saturation magnetization (M_s) and Coercivity (H_c) with Composition (x). Figure clearly reveals soft ferrite (temporary magnet)-like behavior of foldable sheets. The magnetic findings in flexible mats of $_x$(PU/PMMA IPN)-$_{1-x}$($Ba_{0.5}Sr_{0.5}Fe_{12}O_{19}$ hexagonal ferrite nanoparticles) such as saturation magnetization (M_s), remnant magnetization (M_r) and coerecivity (H_c) along with Anisotropy Constant and square-ness ratio (M_r/M_s) calculated from curves have been reported in Table *4*.

How to cite this article:
Kumar A, . G, Jakhar N (September 23, 2026) Interfacial Engineering of Polyurethane and Polymethyl Methacrylate Interpenetrating Polymer Networks using Hexaferrite Nanoceramics for Enhanced Magneto-Dielectric and Thermo-Mechanical Properties. Cureus J Eng 3 : es44388-026-00289-y. DOI https://doi.org/10.7759/s44388-026-00289-y

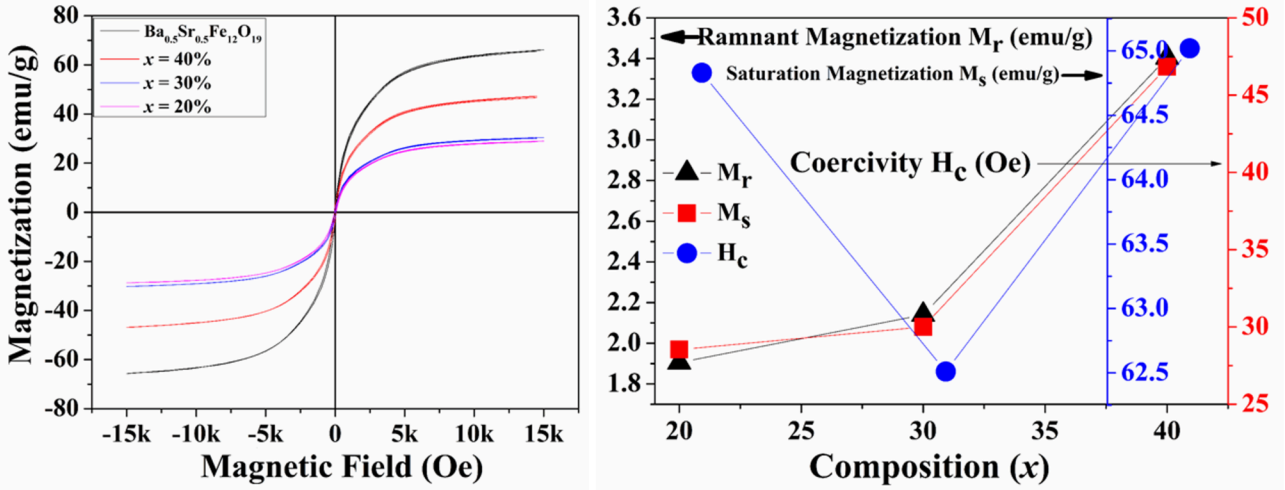


FIGURE 4: Magnetization (emu/g) vs. applied magnetic field (Oe) of flexible mats of x(PU/PMMA IPN)-1-x(Ba0.5Sr0.5Fe12O19 hexagonal ferrite nanoparticles, where x = 20%, 30%, 40%)

PU, Polyurethane; PMMA, Polymethyl Methacrylate; IPN, Interpenetrating Polymer Network

Composition (x)	M_r (emu/g)	M_s (emu/g)	H_c (Oe)	Anisotropy Constant = M_w = Molecular Weight Ms = Saturation Magnetization	M_r/M_s Squareness Ratio
$Ba_{0.5}Sr_{0.5}Fe_{12}O_{19}$	4.208	65.34	64.42	4384.58	0.065
x = 40%	3.404	46.84	65.02	3172.43	0.072
x = 30%	2.140	30	62.51	1953.43	0.071
x = 20%	1.905	28.54	64.83	1927.34	0.066

TABLE 4: The saturation magnetization (Ms), remnant magnetization (Mr) and coercivity (Hc), anisotropy constant and squareness ratio (Mr/Ms) of flexible mats of x(PU/PMMA IPN)-1-x(Ba0.5Sr0.5Fe12O19 hexagonal ferrite nanoparticles, where x = 20%, 30%, 40%)

PU, Polyurethane; PMMA, Polymethyl Methacrylate; IPN, Interpenetrating Polymer Network

It has been clearly analyzed from the table that both saturation magnetization as well as remnant magnetization decrease with decreasing stoichiometric proportion of filler ($Ba_{0.5}Sr_{0.5}Fe_{12}O_{19}$) in the matrix of PU-PMMA entangled polymer. Such response may have resulted due to suppression of the interaction of inter-particle exchange due to nonmagnetic nature of PU/PMMA entangled polymer. The low value of coercivity reveals temporary magnetic response established due to homo-valent substitution of Sr at the Ba site in hexaferrite. The slight decrease in the value of

coercivity signatures for decreased magneto-crystalline anisotropy response due to the polymer matrix eases domain wall movement as well as the change in transition from rigid pinning to softer magnetic behavior retains hard-magnetic nature, confirming hexaferrite dominance. The lower magnetic alignment with enhanced random orientation of ferrite particles as well as decreased inter-grain coupling has been estimated from the change in square-ness reported in Table *4*, and a value <0.5 indicates ferromagnetic response due to multi-domain behavior. The decrease in anisotropy constant reveals a lower contribution of hexagonal ferrite anisotropy due to the polymer chains reducing effective anisotropic energy density. The occupancy of substituent also strongly influenced the magnetic response of hexaferrite nanoparticles due to tetrahedral (d1, d2, d3, d4) site preference occupation. This site of preference occupation is important for magnetic behavior of M-type hexaferrite and octahedral (d7, d8, d9) occupancy. Preferred orientation along the c-axis may result due to tetrahedral occupancy, whereas d0, d5 and d10 did not prefer any site. The atomic size of substituent also strongly affects the preference of occupation. So, average crystallite size also affects magnetic properties. The small value of coercivity (Hc) makes these materials suitable candidates for transformer manufacturing because low coercivity (Hc) allows easy magnetization without low magnetic loss. Saturation magnetization Ms can also increase due to the enlargement of the hyperfine field at 2b and 12k sites as a result of consolidation of Fe^{3+}-O-Fe^{3+}superexchange interaction, which gives the higher net magnetization. The change in value of H_c is due to substitution which changes uniaxial anisotropy constant at $4f_2$ and 2b sites.

To further investigate domain wall movement as well as the change in transition from rigid pinning to softer magnetic behavior that retains hard-magnetic nature, the law of saturation approximation has also been applied for field dependence of magnetization to estimate saturation magnetization ($\boldsymbol{\sigma s}$), anisotropy field (H_a) and effective crystalline anisotropy constant (K_{eff}), where magnetization as a function of magnetic field is given as Equation (6):

$$\sigma s = s\left(1 - \frac{A}{H} - \frac{B}{H^2}\right) + \chi pH \quad (6)$$

Where A is an inhomogeneity constant, B is the magneto-crystalline anisotropy constant and χ is differential susceptibility at high fields (parameters A and c are neglected). The linear fitting of the magnetization ($\boldsymbol{\sigma s}$) as a function of H-2 graph between 1.0 and 1.5 T (10kOe) can be used to estimate $\boldsymbol{\sigma s}$ from an intercept of linear fit at zero field and the slope gives $\boldsymbol{\sigma s} \times$ B [Stoner-Wohlfarth model] and is shown in Figure *5* and the observed values are reported in Table *5*.

How to cite this article:
Kumar A, . G, Jakhar N (September 23, 2026) Interfacial Engineering of Polyurethane and Polymethyl Methacrylate Interpenetrating Polymer Networks using Hexaferrite Nanoceramics for Enhanced Magneto-Dielectric and Thermo-Mechanical Properties. Cureus J Eng 3 : es44388-026-00289-y. DOI https://doi.org/10.7759/s44388-026-00289-y

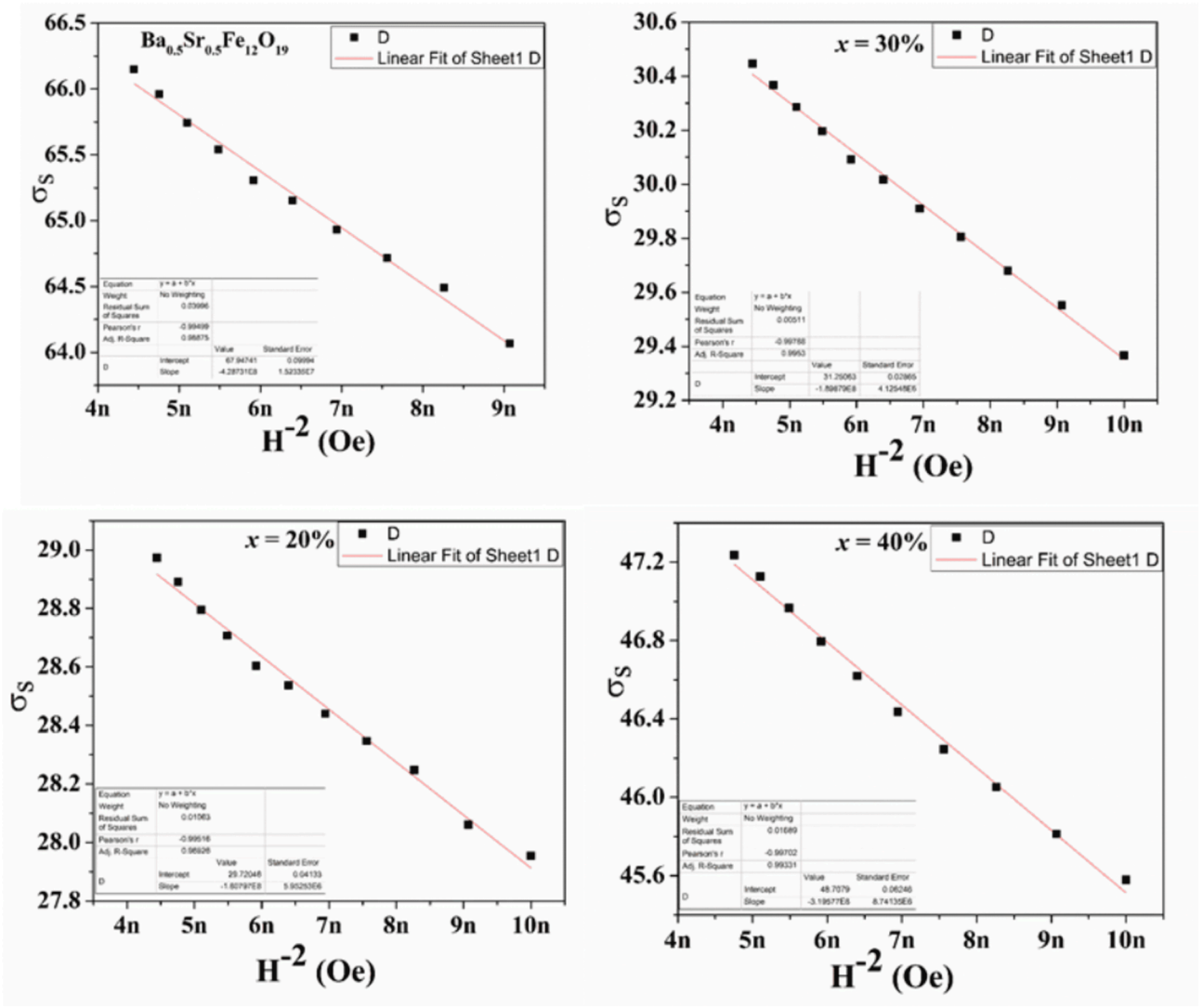


FIGURE 5: Linear fitting σs vs. H-2 (Oe) of flexible mats of x(PU/PMMA IPN)-1-x(Ba0.5Sr0.5Fe12O19 hexagonal ferrite nanoparticles, where x = 20%, 30%, 40%)

PU, Polyurethane; PMMA, Polymethyl Methacrylate; IPN, Interpenetrating Polymer Network

Composition (x)	B (Oe^2)	s_s (emu/g)	K_{eff}	H_a (Oe)
$Ba_{0.5}Sr_{0.5}Fe_{12}O_{19}$	6.129×10^6	67.94	335.33×10^3	9.629×10^3
x = 40%	6.561×10^6	48.70	243.24×10^3	9.987×10^3
x = 30%	6.075×10^6	31.25	149.15×10^3	9.54×10^3
x = 20%	6.083×10^6	29.72	141.94×10^3	9.55×10^3

TABLE 5: Keff, B (Oe2), Ha (Oe), σs (emu/g) of flexible mats of x(PU/PMMA IPN)-1-x(Ba0.5Sr0.5Fe12O19 hexagonal ferrite nanoparticles, where x = 20%, 30%, 40%)

PU, Polyurethane; PMMA, Polymethyl Methacrylate; IPN, Interpenetrating Polymer Network

Using the value of intercept and slope, an effective magnetic crystalline anisotropy coefficient (K_{eff}) can be calculated using evaluated anisotropy constant (B) for the hexagonal structure as given in Equation (7):

$$B = \frac{4K_{eff}^2}{15\sigma^2 s} (7)$$

4/15 is a constant value considered for magneto-crystalline anisotropy along the easy axis of magnetization in M-type hexaferrite. The anisotropy field (H_a) and an effective magnetic crystalline anisotropy coefficient (K_{eff}) are related as given in Equation (8):

$$H_a = \frac{2K_{eff}}{\sigma s} (8)$$

It has been reported that in Sr modified Ba-M hexaferrite, saturation magnetization decreases from ss ~ 67.94 to 29.72 emu/g, and the anisotropy field (Ha) first increases from 9.629 × 103 to 9.987 × 103 and then decreases to 9.55 × 103 at room temperature. Our results of ss are very much similar to reported values. These smaller values of coercivity (H_c = ~ 64.42, 65.02, 62.51, and 64.83 Oe) for prepared foldable and flexible mats of $_x$(PU/PMMA IPN)-$_{1-x}$($Ba_{0.5}Sr_{0.5}Fe_{12}O_{19}$ hexagonal ferrite nanoparticles, where x = 20%, 30%, 40%) clearly reveal maximum efficiency for magnetizing/demagnetizing responsible for sensing of moving currents that leads to a magnetic field for storage applications. The values of effective magnetic crystalline anisotropy coefficient (K_{eff}) decrease from 335.33×10^3 to 141.94×10^3 [29-32], possessing magnetic softness to crystal anisotropy. This decrease in the value of effective magnetic crystalline anisotropy coefficient (K_{eff}) is responsible for the decreased contribution of hexagonal anisotropy due to reduced effective anisotropic energy density, internal magnetic density, and wall pinning strength due to the long-chain polymer. The coercivity of the ferrite system is on account of magnetocrystalline and shape anisotropy and also due to grain size, as given below in Equation (9):

$$H_c = 0.48\left[\left(\frac{2K_{\text{eff}}}{\mu_0 \sigma s}\right) - N\sigma s\right] (9)$$

$\mu 0$ is the permeability of free space, N is the demagnetizing factor and σs is the saturation magnetization. The coercivity of our Magnetic and Dielectric Hexagonal Ceramic Oxides increases slightly from 62.85 to 75.33 Oe, suggesting only slight increase in the crystalline anisotropy along easy axis of magnetization with single domain structure, rather the multi-domain structure. The critical size of single domain grain is estimated as calculated in Equation (10):

$$d_c = \frac{9\epsilon w}{2\pi\sigma^2 s} (10)$$

Impact of incorporation of ceramic inorganic filler (Ba0.5Sr0.5Fe12O19 hexagonal ferrite nanoparticles) in the matrix of entangled PU-PMMA interpenetrating polymer network has been analyzed from mechanical testing such as elongation at break as well as hardness. For this, tensile strength and elongation at break along with hardness of flexible mats of $_x$(PU/PMMA IPN)- $_{1-x}$($Ba_{0.5}Sr_{0.5}Fe_{12}O_{19}$ hexagonal ferrite nanoparticles), where x = 20%, 30%, 40% has been recorded by using Instron 30 tensile tester running at 51 RPM speed and measured values of tensile strength and elongation at break have been tabulated in Table *6*. This table clearly indicates that tensile strength and elongation at break first increase and then decrease with continuous increase in loading ($Ba_{0.5}Sr_{0.5}Fe_{12}O_{19}$ hexagonal ferrite nanoparticles in the matrix of entangled PU-PMMA) results in the optimized concentration of loading in the matrix of PU-PMMA IPN being maximum for x = 30%, although magnetic and dielectric properties increase with increasing loading. The decrease in value of elongation at x = 40% is responsible for the decrease in polymeric behavior of flexible mats. The reason for the increase in elongation at break may result due to exfoliation of ceramic filler used in nanocomposites, and chain interconnectivity generated by ceramic filler enhanced the chain interconnectivity.

Composition (x)	Thickness (mm)	Elongation at Break (%)	Tensile Strength at Break (KG/cm^2)
x = 40%	6.561×10^6	55.70	2.89
x = 30%	6.075×10^6	69.25	9.78
x = 20%	6.083×10^6	83.72	18.95

TABLE 6: Elongation at break, tensile strength, and thickness of flexible mats of x(PU/PMMA IPN)-1-x(Ba0.5Sr0.5Fe12O19 hexagonal ferrite nanoparticles), where x = 20%, 30%, and 40%

PU, Polyurethane; PMMA, Polymethyl Methacrylate; IPN, Interpenetrating Polymer Network

The enhancement in dielectric properties such as ε', ε" and σs vs. frequency due to incorporation of inorganic ceramic as filler ($Ba_{0.5}Sr_{0.5}Fe_{12}O_{19}$ hexagonal ferrite nanoparticles) for improving mechanical strength has been studied using impedance analyzer at room temperature. ε' and ε" vs. frequency at room temperature of flexible mats of x(PU/PMMA IPN)- 1-x($Ba_{0.5}Sr_{0.5}Fe_{12}O_{19}$ hexagonal ferrite nanoparticles, where x = 20%, 30%, 40% have been shown in Figure *5*. The graphs clearly reveal that value of dielectric constant (ε' and ε") decreases with increasing frequency, corresponding to

the presence of normal Debye response. The dielectric constant decreases very sharply up to certain value and then becomes constant (higher value of both real and imaginary part of dielectric permittivity in lower frequency regime) leads to dielectric dispersion, which means deviation from normal Debye response. This dielectric dispersion may result due to the dipole's inactive behavior when external electric field (ac electric field) is applied for contributing to the dielectric constant. As frequency changes, change in valence state of cations and space charge polarization are responsible for the decrease of dielectric constant. It has been clearly visualized from Figure *5* that both real and imaginary parts of dielectric permittivity increase with increasing wt% of inorganic filler ($Ba_{0.5}Sr_{0.5}Fe_{12}O_{19}$ hexagonal ferrite nanoparticles). In lower frequency range, the value of real and imaginary parts of dielectric (ε′ and ε″) must be due to the contribution of dipolar and interfacial polarization along with electronic and ionic polarization, whereas elimination of the contribution of interfacial polarization decreases dielectric properties, and such type of response has been explained on the basis of Koop's theory as well as Maxwell-Wagner-Sillars interfacial polarization, which becomes dominant in heterogeneous systems consisting of conductive fillers dispersed in an insulating matrix. The large contrast in electrical conductivity and permittivity between the ferrite nanoparticles and the PU/PMMA IPN leads to charge accumulation at the polymer-ferrite interfaces under an applied alternating electric field. As the filler concentration increases, the number of such interfaces rises significantly, resulting in enhanced space-charge polarization and, consequently, higher dielectric constant values. According to this theory, dielectric properties mainly depend upon conducting grains and grain boundaries (low permittivity region) [33-36], as well as the increase in dielectric constant can be explained on the basis of the presence of Fe^{3+}/Fe^{2+} ions in $Ba_{0.5}Sr_{0.5}Fe_{12}O_{19}$ hexagonal ferrite nanoparticles, which facilitates localized electron hopping mechanisms, which further contribute to polarization at lower and intermediate frequencies. At higher filler loadings (x = 40%), partial formation of micro-capacitive networks within the polymer matrix also enhances the effective dielectric response of the composite mats

In room temperature dielectric profile, relaxation peaks predominantly appear at higher frequency with increasing ferrite content, which directly points toward non-Debye behavior of prepared MF ceramic composites.

$$\epsilon'(\omega) = \epsilon_\infty + (\epsilon_s - \epsilon_\infty)\frac{1 + (\omega\tau_0)^{1-\alpha}\sin\left(\frac{1}{2}\alpha\pi\right)}{1 + 2(\omega\tau_0)^{1-\alpha}\sin\left(\frac{1}{2}\alpha\pi\right) + (\omega\tau_0)^{2(1-\alpha)}} \quad (11)$$

$$\epsilon''(\omega) = (\epsilon_s - \epsilon_\infty)\frac{(\omega\tau_0)^{1-\alpha}\cos\left(\frac{1}{2}\alpha\pi\right)}{1 + 2(\omega\tau_0)^{1-\alpha}\sin\left(\frac{1}{2}\alpha\pi\right) + (\omega\tau_0)^{2(1-\alpha)}} \quad (12)$$

ε_∞ = dielectric constant measured at high frequency, ε_s = dielectric constant measured at low frequency, $\omega = 2\pi f$ the angular frequency of applied field and τ = characteristic relaxation time of the medium.

The value of α defines the deviation from the Debye model, and it varies from 0 to 1 and also reveals the shape of spectral curves, and for the standard Debye model, α = 0 and the Cole-Cole model reduces to the Debye model. To affirm the presence of non-Debye response, dielectric data have been fitted with the Cole-Cole dielectric relaxation model, and the value of a and b define whether prepared flexible mats of $_x$(PU/PMMA IPN)-$_{1-x}$($Ba_{0.5}Sr_{0.5}Fe_{12}O_{19}$ hexagonal ferrite nanoparticles), where x = 20%, 30%, and 40% exhibit Cole-Cole dielectric relaxation or Cole-Davidson relaxation.

How to cite this article:
Kumar A, . G, Jakhar N (September 23, 2026) Interfacial Engineering of Polyurethane and Polymethyl Methacrylate Interpenetrating Polymer Networks using Hexaferrite Nanoceramics for Enhanced Magneto-Dielectric and Thermo-Mechanical Properties. Cureus J Eng 3 : es44388-026-00289-y. DOI https://doi.org/10.7759/s44388-026-00289-y

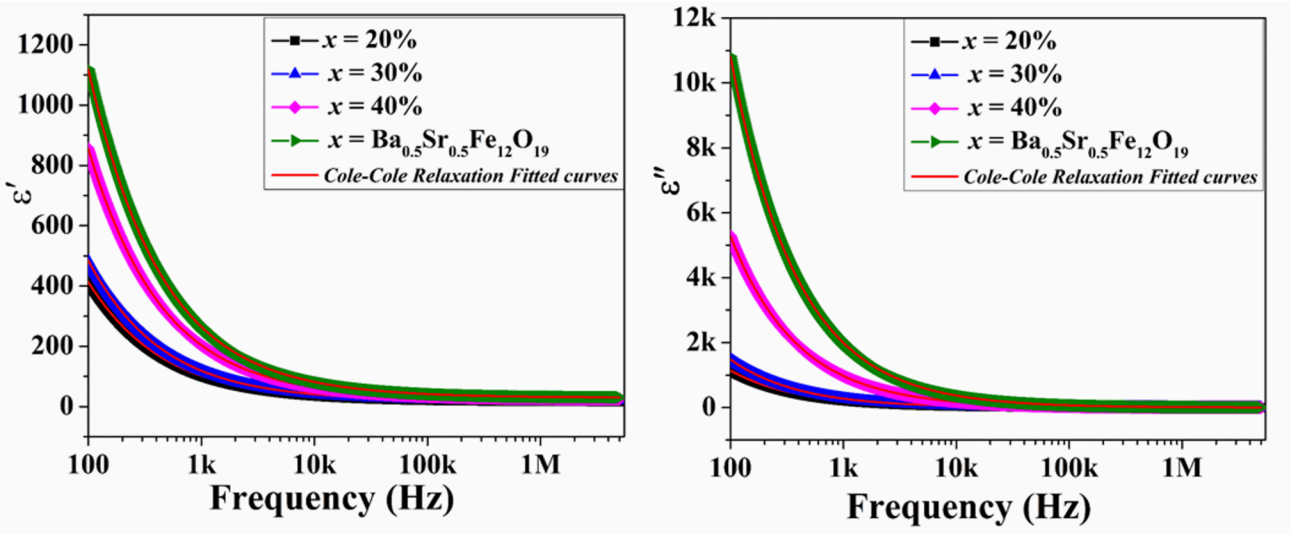


FIGURE 6: Cole-Cole fitting of experimentally collected ε' and ε" vs. frequency of flexible mats of x(PU/PMMA IPN)-1-x(Ba0.5Sr0.5Fe12O19 hexagonal ferrite nanoparticles), where x = 20%, 30%, and 40%

PU, Polyurethane; PMMA, Polymethyl Methacrylate; IPN, Interpenetrating Polymer Network

Composition (x)	For ε' vs. frequency curve		For ε" vs. frequency curve	
	τ	α	τ	α
$Ba_{0.5}Sr_{0.5}Fe_{12}O_{19}$	3.86×10^{-2}	0.35	2.03×10^{-1}	0.27
x = 40%	7.79×10^{-2}	0.36	1.96×10^{-1}	0.27
x = 30%	2.56×10^{-2}	0.27	4.12×10^{-2}	0.25
x = 20%	1.20×10^{-2}	0.30	2.01×10^{-1}	0.28

TABLE 7: Fitted parameters (τ and α) of ε' and ε" vs. frequency obtained from dielectric fitting (Cole-Cole relaxation model) of experimentally collected dielectric data at room temperature of flexible mats of x(PU/PMMA IPN)-1-x(Ba0.5Sr0.5Fe12O19 hexagonal ferrite nanoparticles), where x = 20%, 30%, and 40%

PU, Polyurethane; PMMA, Polymethyl Methacrylate; IPN, Interpenetrating Polymer Network

The value of fitted parameters obtained from fitting such as relaxation time (τ) and (a) are tabulated in Table *7*. (τ) is characteristics of dielectric loss or impedance spectra and exhibits a non-monotonic variation with ferrite concentration, showing an initial increase followed by a decrease as the filler content is further increased. It has been clearly visualized that (τ) first increases and then decreases. This increase must be due to restricted mobility of polymer chain segments and interfacial dipoles caused by strong polymer-ferrite interactions. The embedded nanoparticles act as

physical barriers, increasing dipolar friction and delaying polarization relaxation processes. The enhanced interfacial area at this composition leads to stronger space-charge trapping, which requires longer times to relax under an alternating field.

However, at higher ferrite loading (x = 40%), the initial increase and subsequent decrease of τ must be due to a reduction in the contribution from the formation of interconnected ferrite clusters or quasi-percolative pathways, which facilitate faster charge transport and hopping conduction across interfaces. The increased availability of charge carriers and reduced potential barriers enable quicker polarization-depolarization cycles, thereby shortening the relaxation time. This behavior indicates a transition from dipole-dominated relaxation to interfacial charge-transport-assisted relaxation.

This observed improvement in both real and imaginary parts of dielectric permittivity in lower frequency regime, as well as the non-monotonic variation due to the variation of τ and α, indicates a strong correlation between filler concentration, interfacial polarization, and charge transport dynamics of flexible mats of $_{x}$(PU/PMMA IPN)-$_{1-x}$($Ba_{0.5}Sr_{0.5}Fe_{12}O_{19}$ hexagonal ferrite nanoparticles, where x = 20%, 30%, and 40%. The interplay between polymer chain confinement at low to moderate filler loadings and enhanced charge carrier mobility at higher ferrite contents governs the overall dielectric relaxation behavior.

To analyze the effect of substitution of $Ba_{0.5}Sr_{0.5}Fe_{12}O_{19}$ hexagonal ferrite nanoparticles as inorganic filler in matrix of PU/PMMA IPN, conductivity profile vs. frequency at RT has been studied. Figure *6* shows the frequency dependence of RT recorded electrical conductivity of flexible mats of $_{x}$(PU/PMMA IPN)-$_{1-x}$($Ba_{0.5}Sr_{0.5}Fe_{12}O_{19}$ hexagonal ferrite nanoparticles), where x = 20%, 30%, and 40% . The ac conductivity is calculated from the measured dielectric data using the relation [35]:

$$\sigma_{ac} = 2\pi f \epsilon' \epsilon'' \tan\delta \quad (13)$$

Parameters mentioned in the above formula have their usual meaning. It can be observed that the ac conductivity increases with increasing frequency for all compositions. The ac conductivity profile comprises of two regions marked as frequency independent, corresponding to dc conductivity (σdc), whereas the frequency dependence response, which is also termed as the dispersion region, is called ac conductivity (σac). To retrieve the conduction response, plateau region corresponds to dc conductivity (σ_{dc}) and dispersion region corresponds to ac conductivity (σac) have been studied in detail using the universal principle known as Jonscher's power law [37,38]

$$\sigma dc + Awn = \sigma ac \quad (14)$$

Where "A" represents the dispersion parameter representing the strength of polarizability and "n" is the dimensionless frequency exponent representing the interaction between mobile ions and the lattice around them. According to Jonscher, the origin of the frequency dependence of conductivity lies in the relaxation phenomenon arising due to hopping of mobile charge carriers. Thus, with increasing concentration of oxygen vacancies, the concentration of structural defects increases and hence the value of conductivity increases (Figure *7*).

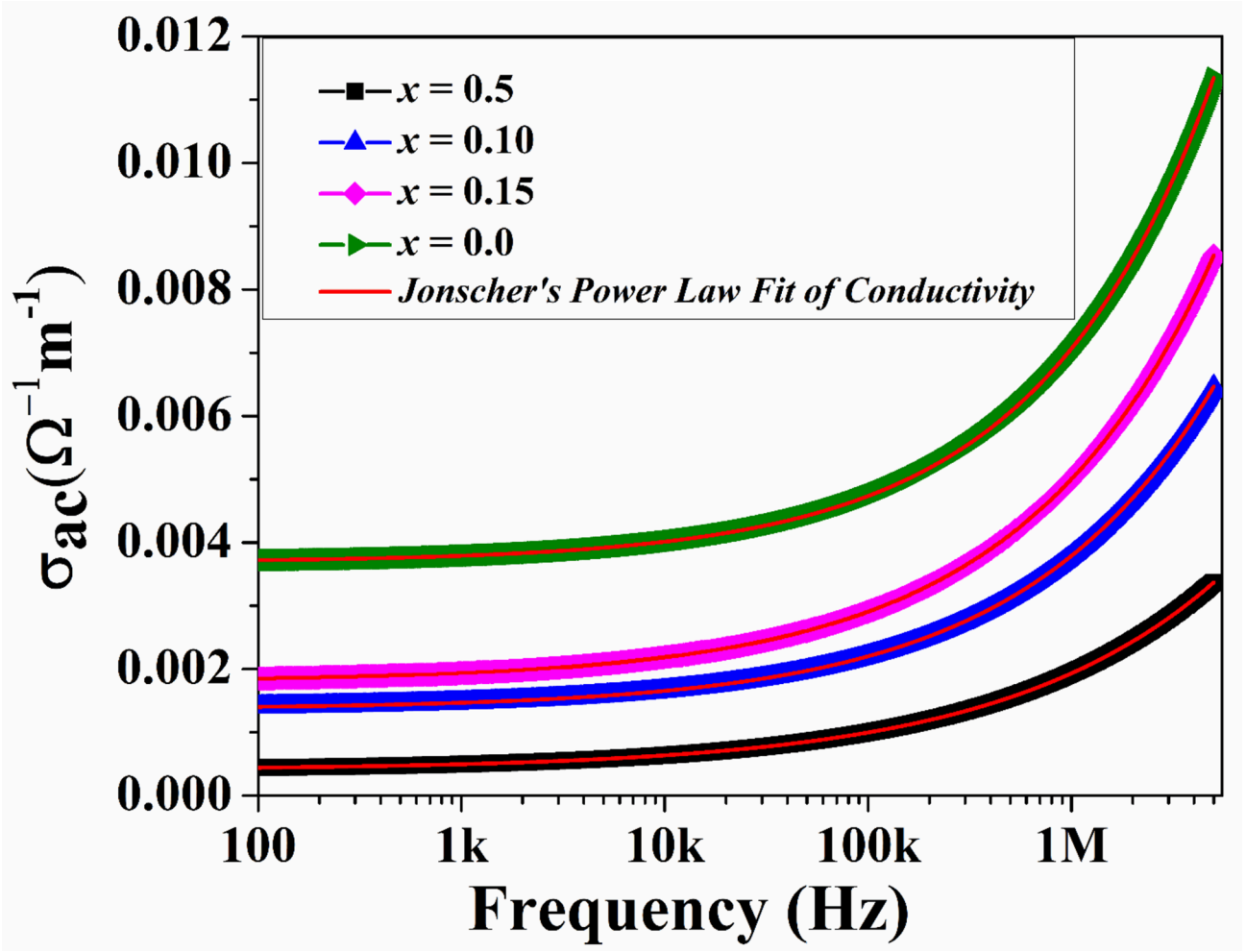


FIGURE 7: Room temperature ac conductivity (σac) vs. frequency of flexible mats of x(PU/PMMA IPN)- 1-x(Ba0.5Sr0.5Fe12O19 hexagonal ferrite nanoparticles, where x = 20%, 30%, 40%

PU, Polyurethane; PMMA, Polymethyl Methacrylate; IPN, Interpenetrating Polymer Network

Composition	n	A (S $cm^{-1}S^n$)	s_{dc} (Scm^{-1})
$Ba_{0.5}Sr_{0.5}Fe_{12}O_{19}$	0.5085	3.0045 10^{-6}	0.00369
x = 40%	0.4699	4.7711 10^{-6}	0.00185
x = 30%	0.4624	4.0706 10^{-6}	0.00137
x = 20%	0.4119	5.1608 10^{-6}	0.00041

TABLE 8: Fitted parameters (n, A, and σdc) of σac vs. frequency obtained from dielectric fitting (Jonscher's power law) of experimentally collected dielectric data at room temperature of flexible mats of x(PU/PMMA IPN)-1-x(Ba0.5Sr0.5Fe12O19 hexagonal ferrite nanoparticles), where x = 20%, 30%, and 40%

PU, Polyurethane; PMMA, Polymethyl Methacrylate; IPN, Interpenetrating Polymer Network

It has been clearly seen from Table *8* that dc conductivity (σdc) decreases from 0.00369 to 0.00185 for $Ba_{0.5}Sr_{0.5}Fe_{12}O_{19}$ in flexible mats of $_x$(PU/PMMA IPN)- $_{1-x}$($Ba_{0.5}Sr_{0.5}Fe_{12}O_{19}$ hexagonal ferrite nanoparticles), where x = 40%. This decrease may result due to 60% contribution of non-conducting nature of the flexible mats of PU/PMMA IPN. It has been discovered that the value of n varies between 0.50 and 0.46. A value of n < 1 indicates that the sample's charge carriers undergo a translational motion that includes abrupt hopping.

Conclusions

Present research entitles 'Investigation of Magnetic, Mechanical, and Dielectric Properties of Hexaferrite-Modified PU/PMMA Interpenetrating Polymer Networks (IPNs)' investigates establishment of magnetic and dielectric response in hybrid composites of Ceramic-Entangled Polymer Network. The interpenetrating polymer network of two entangled polymer starting from their monomers (PU and PMMA) has been prepared using sequential polymerization along with subsequently modified with controlled loadings (As per stoichiometric response) of hexaferrite nano-ceramic ($Ba_{0.5}Sr_{0.5}Fe_{12}O_{19}$) as inorganic fillers. The presence of inorganic filler $Ba_{0.5}Sr_{0.5}Fe_{12}O_{19}$ has been confirmed from XRD with peak positions appearing at 2θ ~ 32.41 and 34. 23 in experimentally collected data of foldable sheet, confirming the presence of hexagonal structural phase of M-type hexaferrite ($SrBaFe_{12}O_{19}$), whereas broad diffraction peak from 2θ ~12° to 20° must be due to polymer nature of PU-PMMA IPN.

Whereas, the microstructure studied from scanning electron microscopy reveals that the white region in micrographs reveals $Ba_{0.5}Sr_{0.5}Fe_{12}O_{19}$ hexagonal ferrite nanoparticles of ceramics in PU-PMMA foldable flexible mats. The magnetic hysteresis shows a decrease in saturation magnetization from 65.34 emu/g for $Ba_{0.5}Sr_{0.5}Fe_{12}O_{19}$ to 46.34 for x = 40%, which may result due to nonmagnetic response of PU/PMMA IPN, and the increase in magnetization with increasing loading upto $Ba_{0.5}Sr_{0.5}Fe_{12}O_{19}$ x = 40%. The high magneto-crystalline anisotropy, due to hexaferrites results in the consideration of Flexible Mats of $_x$(PU/PMMA IPN)- $_{1-x}$($Ba_{0.5}Sr_{0.5}Fe_{12}O_{19}$ hexagonal ferrite nanoparticles) for various magnetic-dielectric applications, whereas narrow hysteresis puts these IPN in category of storage device application. The fitting of ε' and ε" vs. frequency shows deviation from normal dielectric (Debye behavior) with the Cole-Cole dielectric relaxation model, and the first increase and then decrease of τ must be due to a reduction in the contribution of the

How to cite this article:
Kumar A, . G, Jakhar N (September 23, 2026) Interfacial Engineering of Polyurethane and Polymethyl Methacrylate Interpenetrating Polymer Networks using Hexaferrite Nanoceramics for Enhanced Magneto-Dielectric and Thermo-Mechanical Properties. Cureus J Eng 3 : es44388-026-00289-y. DOI https://doi.org/10.7759/s44388-026-00289-y

formation of interconnected ferrite clusters or quasi-percolative pathways, which facilitate faster charge transport and hopping conduction across interfaces. The Jonscher's power law fitting of conductivity data shows an increase in dc conductivity of flexible mats due to the increase in loading of ($Ba_{0.5}Sr_{0.5}Fe_{12}O_{19}$) in the matrix of PU/PMMA IPN.

Additional Information

Author Contributions

All authors have reviewed the final version to be published and agreed to be accountable for all aspects of the work.

Concept and design: Anil Kumar, Gagandeep ., Narendra Jakhar

Acquisition, analysis, or interpretation of data: Anil Kumar, Gagandeep ., Narendra Jakhar

Drafting of the manuscript: Anil Kumar, Gagandeep ., Narendra Jakhar

Critical review of the manuscript for important intellectual content: Anil Kumar, Gagandeep ., Narendra Jakhar

Supervision: Gagandeep ., Narendra Jakhar

Disclosures

Human subjects: All authors have confirmed that this study did not involve human participants or tissue.

Animal subjects: All authors have confirmed that this study did not involve animal subjects or tissue.

Conflicts of interest: In compliance with the ICMJE uniform disclosure form, all authors declare the following:

- **Payment/services info:** All authors have declared that no financial support was received from any organization for the submitted work.
- **Financial relationships:** All authors have declared that they have no financial relationships at present or within the previous three years with any organizations that might have an interest in the submitted work.
- **Other relationships:** All authors have declared that there are no other relationships or activities that could appear to have influenced the submitted work.

Data Availability Statements

The datasets (and/or code) supporting this study are available from the corresponding author upon reasonable request.
All data generated or analyzed during this study are included in this published article and/or its appendices.
Data sharing is not applicable. This work is theoretical; no datasets were generated or analyzed.

References

1. Lee DK, Tsai HB: Properties of segmented polyurethane derived from different diisocyanate. Journal of Applied Polymer Science. 2000, 75:167-174. 10.1002/(SICI)1097-4628(20000103)75:1<167::AID-APP19>3.0.CO;2-N

2. Jeevananda T, Begum M, Siddaramaiah: Studies on polyaniline filled PU/PMA interpenetrating polymer networks. European Polymer Journal. 2001, 37:1213-1218. 10.1016/s0014-3057(00)00228-7

3. Cao X, Lee LJ, Widya T, Macosko C: Polyurethane/clay nanocomposites foams: processing, structure and properties. Polymer. 2005, 46:775-783. 10.1016/j.polymer.2004.11.028

4. Chen S, Wang Q, Wang T: Physical properties of a high molecular weight hydroxyl-terminated polydimethylsiloxane modified castor oil based polyurethane/epoxy interpenetrating polymer network composites. Applied Physics A. 2010, 103:1047-1052. 10.1007/s00339-010-6034-0

5. Mathew AP, Packirisamy S, Radusch HJ, Thomas S: Effect of initiating system, blend ratio and crosslink density on the mechanical properties and failure topography of nano-structured full-interpenetrating polymer networks from natural rubber and polystyrene. European Polymer Journal. 2001, 37:1921-1934. 10.1016/s0014-3057(01)00067-2

6. Parthiban S, Ragunandan BN, Jain SR: Interpenetrating polymer networks as binders for solid composite propellants. Defence Science Journal. 1992, 42:147-156. 10.14429/dsj.42.4374

7. Chen CH, Ma CCM: Pultruded fibre-reinforced PMMA/PU IPN composites: processability and mechanical properties. Composites Part A: Applied Science and Manufacturing. 1997, 28:65-72. 10.1016/s1359-835x(96)00096-6

8. Król P: Generalization of kinetics in the reaction of isocyanates and polyols for modeling a process-yielding linear polyurethane, 1. Journal of Applied Polymer Science. 1995, 57:739-749. 10.1002/app.1995.070570609

9. Kong X, Narine SS: Physical properties of polyurethane plastic sheets produced from polyols from canola oil. Biomacromolecules. 2007, 8:2203-2209. 10.1021/bm070016i

10. Frisch KC, Reegen SL, Thir B: Kinetics of alcohol and polyether polyol-isocyanate reactions using metal catalysts. Journal of Polymer Science Part C: Polymer Symposia. 1967, 16:2191-2201. 10.1002/polc.5070160433

11. Frisch KC, Reegen SL, Floutz WV, Oliver JP: Complex formation between catalysts, alcohols, and isocyanates in the preparation of urethanes. Journal of Polymer Science Part A-1: Polymer Chemistry. 1967, 5:35-42. 10.1002/pol.1967.150050104

12. Frisch KC, Rumao LP: Catalysis in isocyanate reactions. Journal of Macromolecular Science. 1970, 5:103-149. 10.1080/15583727008085365

13. Narine SS, Kong X, Bouzidi L, Sporns P: Physical properties of polyurethanes produced from polyols from seed oils: I. elastomers. Journal of the American Oil Chemists Society. 2007, 84:55-63. 10.1007/s11746-006-1006-4

14. Lligadas G, Ronda JC, Galià M, Cádiz V: Polyurethane networks from fatty-acid-based aromatic triols: synthesis and characterization. Biomacromolecules. 2007, 8:1858-1864. 10.1021/bm070157k

15. Oprea S: Synthesis and properties of polyurethane elastomers with castor oil as crosslinker. Journal of the American Oil Chemists Society. 2009, 87:313-320. 10.1007/s11746-009-1501-5

16. Xu Y, Petrovic Z, Das S, Wilkes GL: Morphology and properties of thermoplastic polyurethanes with dangling chains in ricinoleate-based soft segments. Polymer. 2008, 49:4248-4258. 10.1016/j.polymer.2008.07.027

17. Joshi H, Kumar AR: Investigations and correlations of structural, magnetic, and dielectric properties of M-type barium hexaferrite (BaFe12O19) for hard magnet applications. Journal of Superconductivity and Novel Magnetism. 2022, 35:2435-2451. 10.1007/s10948-022-06203-x

18. Semaida AM, Darwish MA, Salem MM, et al.: Impact of Nd3+ substitutions on the structure and magnetic properties of nanostructured SrFe12O19 hexaferrite. Nanomaterials. 2022, 12:3452. 10.3390/nano12193452

19. Kaynar MB, Özcan Ş, Shah SI: Synthesis and magnetic properties of nanocrystalline BaFe12O19. Ceramics International. 2015, 41:11257-11263. 10.1016/j.ceramint.2015.05.078

20. Kumar S, Bhat SA, Chaurasiya S, Lone GA, Rashid A, Sharma PK, Ikram M: Investigation on the structural, morphological and magnetic properties of Ca1-Eu Fe12-Ti O19 hexaferrite system. Solid State Sciences. 2023, 145:107337. 10.1016/j.solidstatesciences.2023.107337

21. Rather GH, Ikram M: Magnetoelectric coupling in terbium doped particulate multiferroic composites based on BaTiO3-CoFe2O4. Physica B: Condensed Matter. 2020, 599:412577. 10.1016/j.physb.2020.412577

22. Bhat SA, Rashid A, Majeed M, Tantray AM, Rani A, Yousuf S, Ikram M: Enhanced magnetic, ferroelectric, and photocatalytic properties of Nd and Co doped bismuth ferrite (Bi1−xNdxFe1−yCoyO3) ceramics. Inorganic Chemistry Communications. 2024, 170:113148. 10.1016/j.inoche.2024.113148

23. Rather GH, Ikram M: Enhancement of magnetoelectric effect in multiferroic composites of dysprosium and zinc doped BaTiO3-CoFe2O4. Journal of Materials Science: Materials in Electronics. 2021, 32:551-566. 10.1007/s10854-020-04838-x

24. Bhat SA, Tantray AM, Ahsan JU, Ikram M: Exploring the supercapacitive potential of Sm3+ doped CoFe2O4 nanoparticles: Enhanced magnetic and dielectric properties. Ceramics International. 2024, 50:26220-26233. 10.1016/j.ceramint.2024.04.362

25. Xu P, Han X, Wang M: Synthesis and magnetic properties of BaFe12O19 hexaferrite nanoparticles by a reverse microemulsion technique. The Journal of Physical Chemistry C. 2007, 111:5866-5870. 10.1021/jp068955c

How to cite this article:
Kumar A, . G, Jakhar N (September 23, 2026) Interfacial Engineering of Polyurethane and Polymethyl Methacrylate Interpenetrating Polymer Networks using Hexaferrite Nanoceramics for Enhanced Magneto-Dielectric and Thermo-Mechanical Properties. Cureus J Eng 3 : es44388-026-00289-y. DOI https://doi.org/10.7759/s44388-026-00289-y

26. Mosleh Z, Kameli P, Ranjbar M, Salamati H: Effect of annealing temperature on structural and magnetic properties of BaFe12O19 hexaferrite nanoparticles. Ceramics International. 2014, 40:7279-7284. 10.1016/j.ceramint.2013.12.068

27. Fasate SK, Raut AV, Rode S, Babrekar MK, Alone ST, Jadhav KM: Synthesis, TGA, structural, and infrared characterization Bafe12o19 nanoparticles. AIP Conference Proceedings. 2021, 2369: 020155. 10.1063/5.0061182

28. El Shater RE, El-Ghazzawy EH, El-Nimr MK: Study of the sintering temperature and the sintering time period effects on the structural and magnetic properties of M-type hexaferrite BaFe12O19. Journal of Alloys and Compounds. 2018, 739:327-334. 10.1016/j.jallcom.2017.12.228

29. Baykal A, Auwal IA, Güner S, Sözeri H: Magnetic and optical properties of Zn 2+ ion substituted barium hexaferrites. Journal of Magnetism and Magnetic Materials. 2017, 430:29-35. 10.1016/j.jmmm.2016.11.062

30. Asiri S, Güner S, Korkmaz AD, et al.: Magneto-optical properties of BaCryFe12–yO19 (0.0 ≤ y ≤ 1.0) hexaferrites. Journal of Magnetism and Magnetic Materials. 2018, 451:463-472. 10.1016/j.jmmm.2017.11.100

31. Ali I, Islam MU, Awan MS, Ahmad M: Effects of Ga-Cr substitution on structural and magnetic properties of hexaferrite (BaFe12O19) synthesized by sol-gel auto-combustion route. Journal of Alloys and Compounds. 2013, 547:118-125. 10.1016/j.jallcom.2012.08.122

32. Ali I, Islam MU, Awan MS, Ahmad M, Ashiq MN, Naseem S: Effect of Tb3+ substitution on the structural and magnetic properties of M-type hexaferrites synthesized by sol-gel auto-combustion technique. Journal of Alloys and Compounds. 2013, 550:564-572. 10.1016/j.jallcom.2012.10.121

33. Kumar M, Yadav KL: Study of dielectric, magnetic, ferroelectric and magnetoelectric properties in the PbMn(x)Ti(1-x)O(3) system at room temperature. Journal of Physics: Condensed Matter. 2007, 19:242202. 10.1088/0953-8984/19/24/242202

34. Cole KS, Cole RH: Dispersion and absorption in dielectrics: alternating current characteristics. Journal of Chemical Physics. 1941, 9:341-351. 10.1063/1.1750906

35. Havriliak S, Negami S: A complex plane representation of dielectric and mechanical relaxation processes in some polymers. Polymer. 1967, 8:161-210. 10.1016/0032-3861(67)90021-3

36. Prakash V, Choudhary SN, Sinha TP: Dielectric relaxation in complex perovskite oxide BaCo1/2W1/2O3. Physica B: Condensed Matter. 2008, 403:103-108. 10.1016/j.physb.2007.08.015

37. Pradhan DK, Behera B, Das PR: Studies of dielectric and electrical properties of a new type of complex tungsten bronze electroceramics. Journal of Materials Science: Materials in Electronics. 2012, 23:779-785. 10.1007/s10854-011-0492-9

38. Jonscher AK: The 'universal' dielectric response. Nature. 1977, 267:673-679. 10.1038/267673a0

How to cite this article:
Kumar A, . G, Jakhar N (September 23, 2026) Interfacial Engineering of Polyurethane and Polymethyl Methacrylate Interpenetrating Polymer Networks using Hexaferrite Nanoceramics for Enhanced Magneto-Dielectric and Thermo-Mechanical Properties. Cureus J Eng 3 : es44388-026-00289-y. DOI https://doi.org/10.7759/s44388-026-00289-y